REPORT DOCUMENTATION PAGE

Form Approved OMB No. 0704-0188

1. REPORT DATE *(DD-MM-YYYY)*	2. REPORT TYPE	3. DATES COVERED *(From – To)*
01-08-2007	Final Report	25 Jul 07 - 02-Feb-10

4. TITLE AND SUBTITLE

Structural Design and Analysis of an Aeroelastic Tailoring and Passive Load Alleviation Concept for a Sensor Craft

5a. CONTRACT NUMBER
FA8655-05-1-3006

5b. GRANT NUMBER

5c. PROGRAM ELEMENT NUMBER

6. AUTHOR(S)

Professor Jonathan E Cooper

5d. PROJECT NUMBER

5d. TASK NUMBER

5e. WORK UNIT NUMBER

7. PERFORMING ORGANIZATION NAME(S) AND ADDRESS(ES)

University of Manchester
Oxford Road
Manchester M13 9PL
United Kingdom

8. PERFORMING ORGANIZATION REPORT NUMBER

N/A

9. SPONSORING/MONITORING AGENCY NAME(S) AND ADDRESS(ES)

EOARD
Unit 4515 BOX 14
APO AE 09421

10. SPONSOR/MONITOR'S ACRONYM(S)

11. SPONSOR/MONITOR'S REPORT NUMBER(S)
Grant 05-3006

12. DISTRIBUTION/AVAILABILITY STATEMENT

Approved for public release; distribution is unlimited. (approval given by local Public Affairs Office)

13. SUPPLEMENTARY NOTES

14. ABSTRACT

This report results from a contract tasking University of Manchester as follows: The Grantee will analytically investigate the use of a passive buckling load alleviation concept for a sensorcraft type wing configuration. The outer wing of the sensor craft design leads to the high aspect ratio, which is very favorable for reduction in fuel consumption and range extension. However, it produces high bending moments stemming from maneuvers or wind gusts. This project will investigate the use of an attachment of the outer wing that will enable passive load alleviation due to the washout deflection of the wingtip. A finite element model will be used to investigate and compare strength behavior as well as the static and dynamic aeroelastic performance. An investigation will be performed to show how the load alleviation features can be installed. A study of the outer wing will be performed to investigate the static aeroelastic behavior, position and attachment stiffness of the device. A divergence and flutter analysis will also be performed, and also a buckling analysis will be made to show that this phenomenon will not occur for limit gust or maneuver loads. An assessment of the overall weight reduction using the alleviation device will be conducted.

15. SUBJECT TERMS
EOARD, Structural Dynamics, Structures, Aeroelasticity

16. SECURITY CLASSIFICATION OF:			17. LIMITATION OF ABSTRACT	18, NUMBER OF PAGES	19a. NAME OF RESPONSIBLE PERSON
a. REPORT	b. ABSTRACT	c. THIS PAGE			SURYA SURAMPUDI
UNCLAS	UNCLAS	UNCLAS	UL	34	19b. TELEPHONE NUMBER *(Include area code)* +44 (0)1895 616021

Structural Design and Analysis of a Passive Load Alleviation Concept for a Sensorcraft

FINAL REPORT

Revised 25th July 2007

EOARD Contract FA 8655-05-1-3006

Professor J. E. Cooper, Professor O. Sensburg, Ms. Piyawan Miller, Simon Miller

Effort Sponsored by the Air Force Office of Scientific Research, Air Force Material Command, USAF, under grant number FA8655-05-1-3006. The U.S. Government is authorized to reproduce and distribute reprints for Government purpose notwithstanding any copyright notation thereon.

I certify that there were no subject inventions to declare during the performance of this grant.

SUMMARY

This report describes the continuation of a work programme [1] for the design, manufacture and testing of a passive load gust alleviation device for use on a sensorcraft structure. The testing of a prototype wind tunnel model is described along with the development of an optimised aeroelastic scaling approach which will be used for the design of a future wind tunnel model.

1. INTRODUCTION

Increasing the aspect ratio of an airplane reduces the induced drag and therefore also fuel consumption, which is a great importance for aerospace vehicles such as Sensorcraft that are designed for long endurance missions. Unfortunately a high aspect ratio also increases the wing bending moment and in case of the Sensorcraft reduces the critical buckling speed. The design root bending moment stems either from manoeuvres or gusts and this gives the critical loading case and consequently leads to higher structural mass to withstand the loads.

One way to reduce these loads is by means of active manoeuvre load control or gust alleviation. This is performed by the movement of the control surfaces through the flight control system but requires a highly redundant system and associated controls technology and power requirements.

The alternative approach is to implement a passive load alleviation system which does not require a control system and can be made failsafe without redundancy requirements. The earlier part of this project investigated the use of a passive device and demonstrated its feasibility analytically on a baseline Sensorcraft model. It was found that it would be possible to reduce the design loads and overall structural weight if such a device was used.

This report describes the work continuing the development of a passive load alleviation system from July 2006 to June 2006 under EOARD contract FA8655-05-1-3006.

A simplified 1:40 elastic Sensorcraft model wing with passive gust alleviation device was designed, manufactured and tested in the low subsonic wind tunnel of MACE (Manchester University). The wind tunnel tests show a reduction of wing deflection up to about 50% by using the gust alleviation device. Further effort was devoted towards developing an aeroelastic scaling optimisation process for the design of the wind tunnel model that is to be tested in the next part of the project.

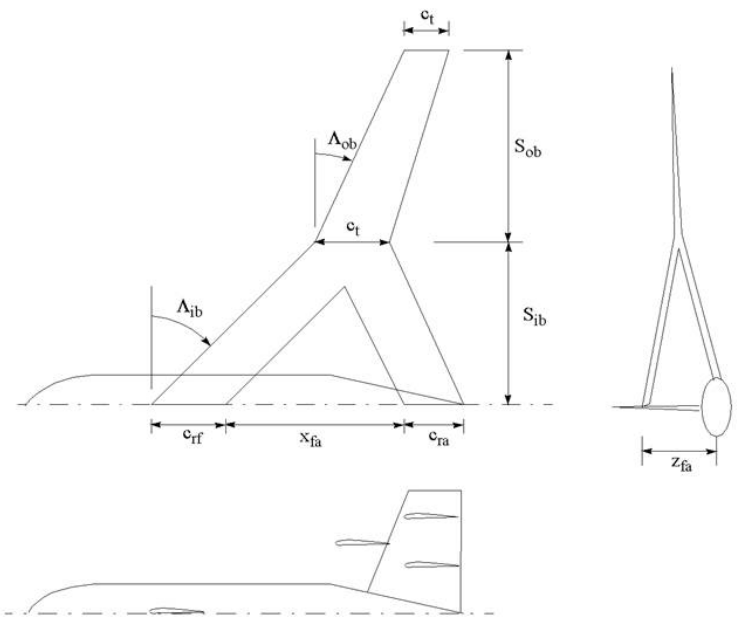

Inboard span	S_{ib}	26m
Outboard span	S_{ob}	8m
Fore Root Chord	C_{rf}	2.5m
Aft Root Chord	C_{ra}	2.5m
Mid-root chord	c_m	2.5m
Inboard Sweep	Λ_{ib}	30 deg
Outboard Sweep	Λ_{ob}	30 deg

Figure 1. Planform Arrangement of Sensorcraft and Baseline Configuration Parameters[2]

2. BASELINE SENSORCRAFT STRUCTURE

The Sensorcraft planform and dimensions used to provide the baseline structure for the scaled prototype wind tunnel model are presented in Figure 1 [2]. It was decided to apply a geometric scaling factor of 40 in order to fit into the wind tunnel that was to be used for testing of the prototype.

2.1. MODEL DIMENSIONS FOR 1:40 MODEL

As can be seen in Figure 1, the total 40th scale model has a span of $\frac{34}{40}$ = 0.85 m and the outer wing gust device $\frac{8}{40}$ = 0.2 m.

2.2. ATTACHMENT SPRING FOR PASSIVE GUST DEVICE

A schematic representation of the gust device can be found is shown in Figure 2. Essentially the wing is ‘cut’ towards the outer tip and both parts are joined via a torque tube along the leading edge. As the outer part is attached well forward of the aerodynamic centre on the quarter chord, the effect of any vertical gust

is to produce a nose down motion in the wing tip, thereby counteracting the effect of gust. As the gust device is at the wing tip, the load alleviation will have a significant effect on the resulting loads.

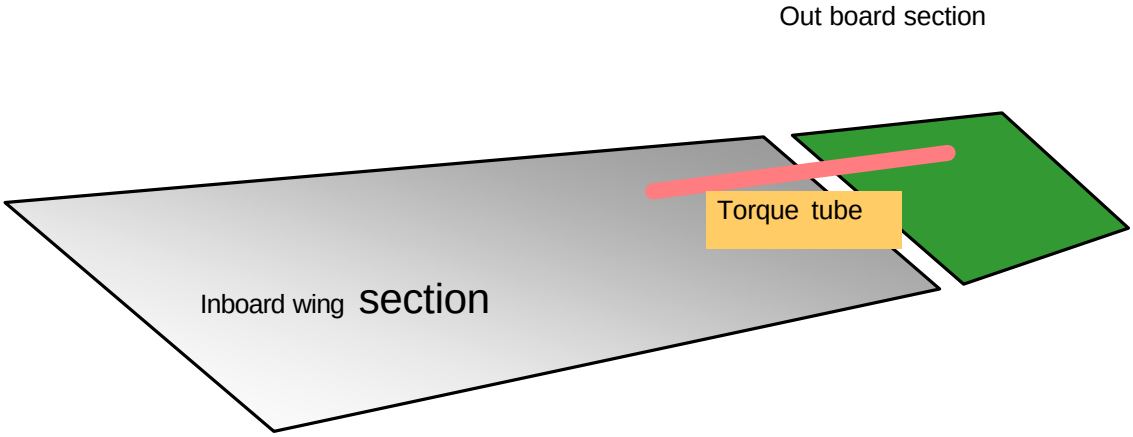

Figure 2. Schematic of Gust Load Alleviation Device

2.2.1. Initial Modeling Approach

The initial approach to confirm the underlying idea behind the passive device was the application of a discrete point loading on the baseline FE wing model which was modified by the introduction of a 'cut' to include the passive device. This single point of action on the outer wing was defined to represent the application of a gust. The resulting washout angle was determined and the consequent discrete gust load after washout could then be defined.

2.2.2. Definition of a Discrete Gust and Point of Action on the Outer Wing

With a gust of 60 ft/sec (=18.15 m/s) at 65 m/s S.L. we get a gust angle of 0.279 rad or 16 degrees. Taking the gust force as:

$$F_z = Ca_a \quad a \ / 57.3 \ q \ F$$

leads to a pressure of $\frac{65^2 1.225}{2}$ = 2.6 KPa and hence the force becomes

4.93 x 0.279 x 2.6 x 20 = 71.5 KN

2.2.3. Modification of Finite Element Model

The outer wing was only attached at the leading edge as shown in Figure 3 along with the position of the discrete gust force. The modification was only applied on the two ribs and the 'nose spar'. The resulting washout angle was calculated from the z displacements of nodes 610 and 591 and 648 and 629 as shown in Figure 4. The resulting washout angle was found to be -6.25 degrees or 0.109 rad. This result can be altered by changing the torsional stiffness of the front spar. A more flexible spar leads to a greater washout and vice versa.

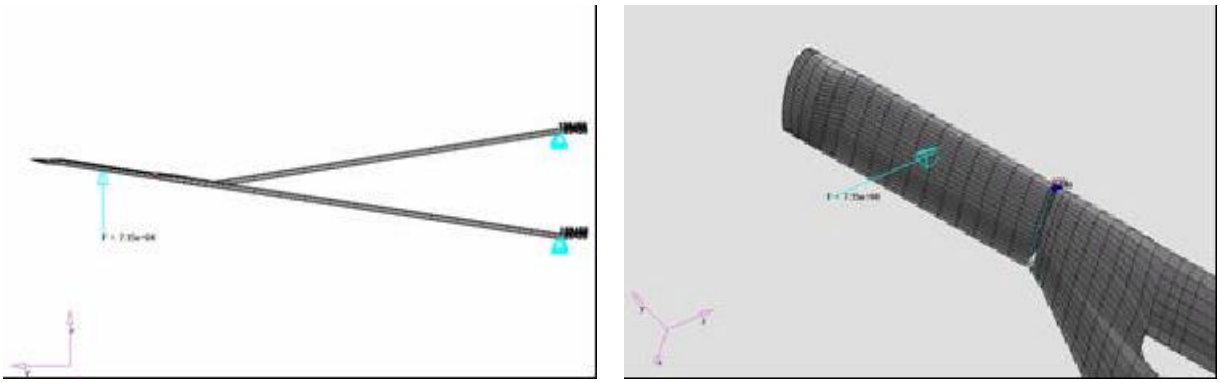

Figure 3. FE Model Showing "Cut" and Point of Discrete Loading

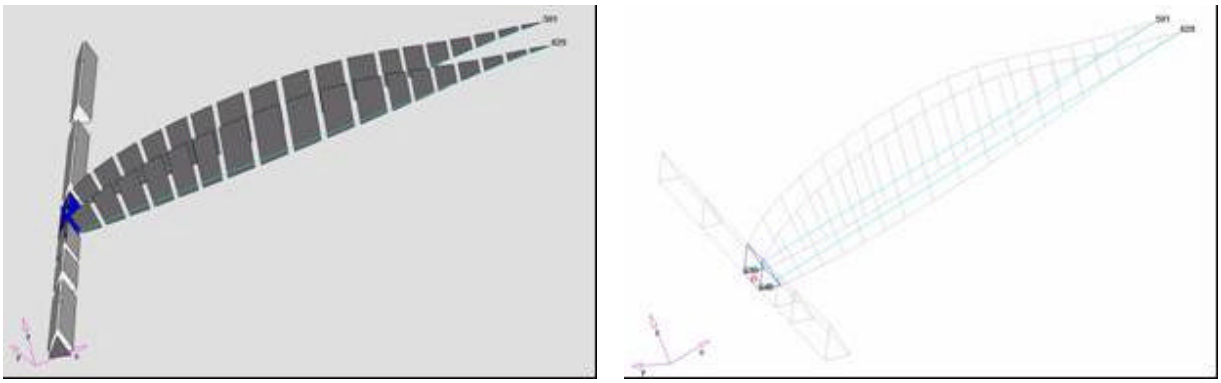

Figure 4. Stiffened structural elements, "leading edge" elements t=40mm, ribs elements t=5mm

From this result the effective torsional stiffness can be deduced using an arm of 0.7 m (distance of outer wing pivot to quarter chord axis) such that

$$K = \frac{M}{\phi} \quad \Rightarrow \quad \frac{71.5 \times 0.7}{0.109} = 459.2 \text{KNm/rad}$$

The equivalent gust angle for a 60 ft/sec gust = 18.15 m/sec is derived as

$\frac{18.15}{65}$ = 0.279 rad = 16 degrees at 65 m/sec.

Therefore an alleviation factor of

$$\frac{0.108_{\text{elastic}}}{0.279_{\text{rigid}}} = 0.39$$

can be calculated.

For the design of the wing tunnel model, we want to achieve a 0.279 rads (16 degrees) rigid gust angle at 25 m/sec, which gives

$$\frac{25^2 \times 1.225}{2} = 0.38\text{KPa}$$

and a vertical force of

4.93 x 0.279 x 0.38 x 20 = 10.45 KN (same wing @ lower speed)

To get 0.109 rad for the elastic sensorcraft at 25 m/sec, the torsional stiffness must be

$\frac{459.2 \times 10.45}{71.5}$ = 67.1 KNm/rad

2.2.4. Wind Tunnel Model 1:40 Scale Spring

Taking 67.1 KNm/rad and multiplying it with $\left(\frac{1}{40}\right)^3$ of Table 1 a stiffness of

67.1 x 0.025^3 = 1.049 Nm/rad results.

Dimensions	Scaling Factor	Units
Length	0.025	Mm
Stiffness	0.025	N/m
Torsional Stiffness	0.025^3	Nm/rad
Frequency	40	Hz
Velocity	1.0	m/s

TABLE 1 SCALE FACTORS

3. MODEL DESIGN

In Figure 5, a picture of wing device / full wing system is shown including rib labeling.

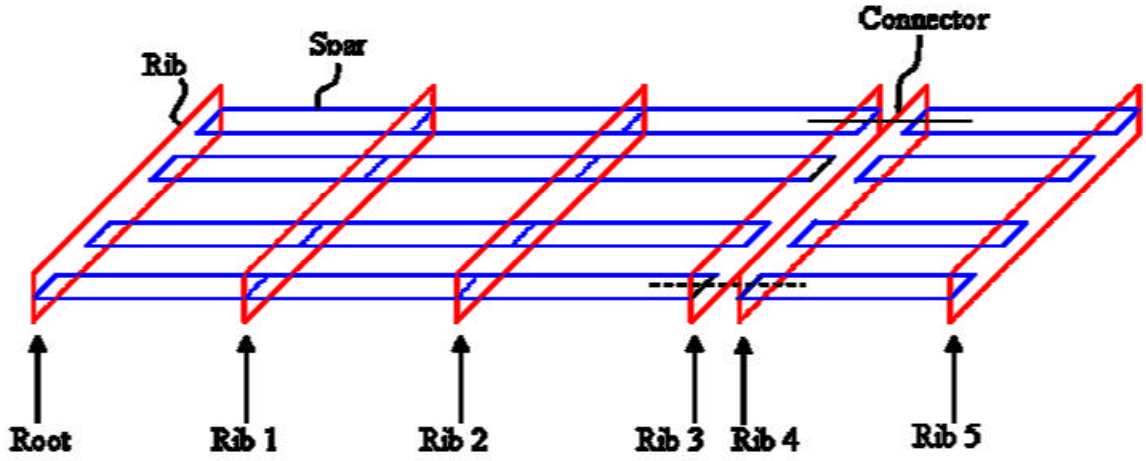

Figure 5 Illustration of Wing-Device/Full Wing system with rib labelling

The dimensions of the wing are presented in Figure 6.

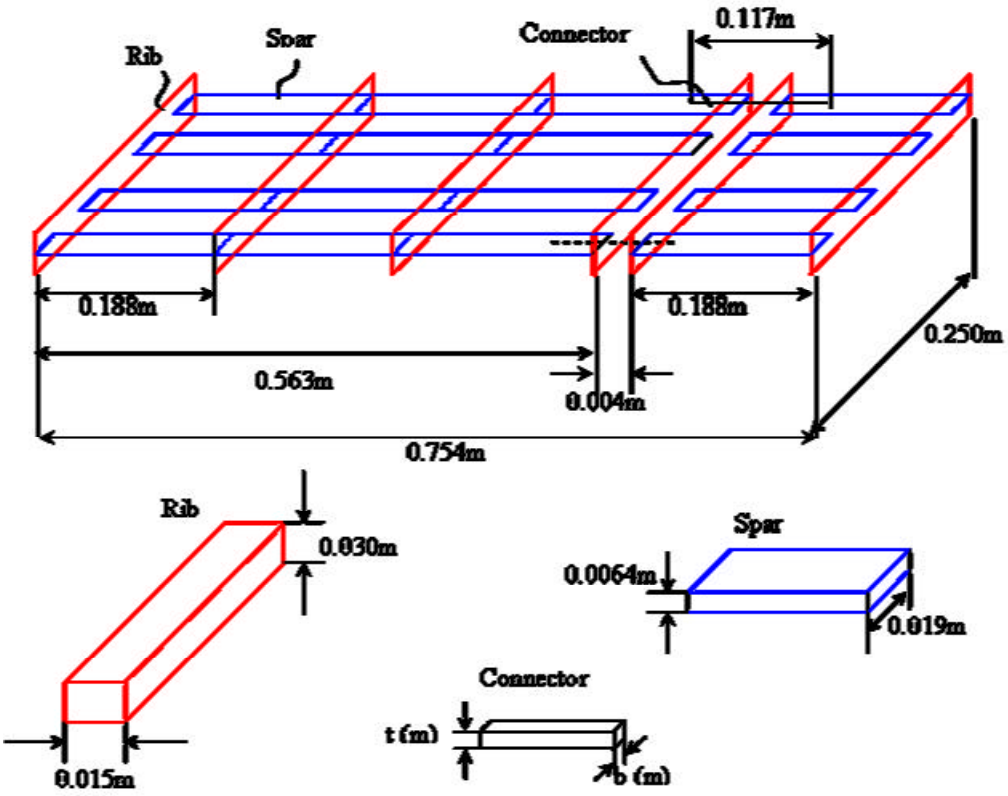

Figure 6. Dimensions of Model With / Without Device

3.1. MANUFACTURE OF WIND TUNNEL WING

3.1.1. Manufacture of the Main Components

It was decided that for the length of the ¾ wing and device, the spars would run straight through each rib from one end to another. This would help the model to maintain its structure when it was not subjected to any loads. In order generate the slots through the ribs, a hole was initially drilled at either end of each slot and was followed by the removal of the remaining material in between using a CNC miller, as shown in Figures 7 and 8.

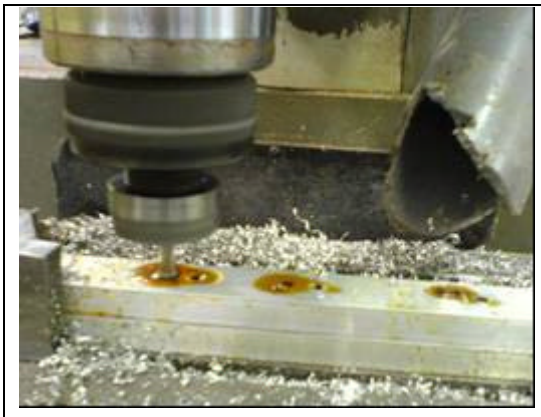

Figure 7. Holes being Drilled in Rib

Figure 8. Milling out material

The ribs were machined from a rectangular aluminum bar using the same CNC miller as above so that they had an aerofoil profile. The profile chosen was the NACA 0012 shown in figure 9. The code '0012' indicates that aerofoil has no camber and a maximum thickness equal to 12% of its chord.

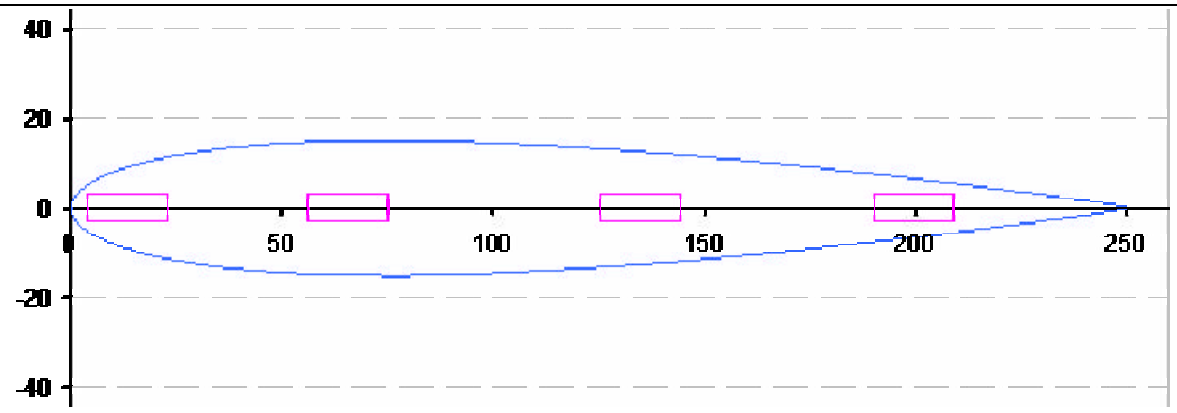

FIGURE 9 NACA 0012 AEROFOIL WITH SPAR POSITION INDICATED

In milling the profile the cutter traced the profile ten times so as to cut through the 15 mm thick block gradually, i.e. with each cycle the cutter increased its depth by 1.5 mm as shown in figures 10 and 11.

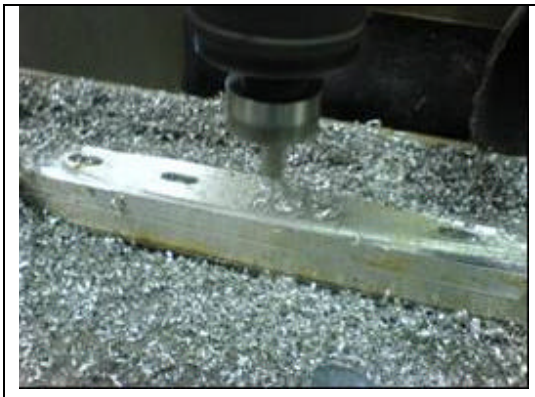

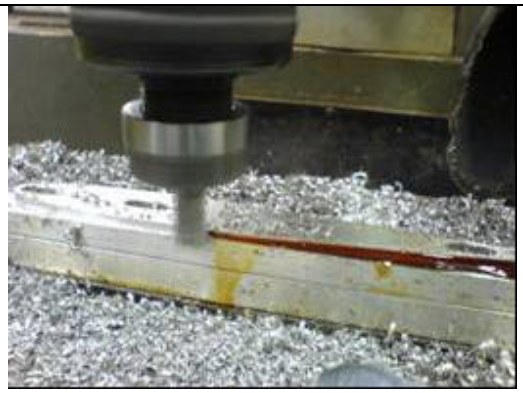

FIGURE 10 PROFILE MILLING OF AEROFOIL SHAPED RIB

FIGURE 11 ORIGINAL BAR AND RIB AFTER MACHINING

Material for the aluminum rectangular spars were ordered in a long bar so that it could be cut down to the correct length.

Holes for the connector were then drilled in the LE and TE spars of the wing and device on the adjacent end faces and the connectors were cut to length from a silver steel rod. Following analytical work, the desired diameter of the connector was known. However, due to material limitations, it was not possible to obtain rods of the required size. The closest two rods were found, one slightly larger and the other smaller, from which the smaller diameter rod was chosen for the current model. By choosing the smaller diameter rod the stiffness of the connector is less than that of the desired diameter.

Prior to assembly of the model, holes were drilled and tapped in four positions along the top surface of the ribs, corresponding to where the spars passed through. Grub screws would then be used as an extra precaution to avoid unwanted movement of the spars and ribs relative to each other. In addition, a further two holes were drilled on the bottom surface of the third and fourth ribs, as well as the LE and TE spars, corresponding to where the connector passes through. Similarly, grub screws were used, but with greater significance, to fix the connector and hence prevent movement at those points.

3.1.2. Manufacture of the Balsa Wood Leading Edge

As the spars are rectangular, an aerofoil shaped leading edge was made from balsa wood. This is to provide support for the solarfilm to be later wrapped around the wing and device, which then constitutes the skin of the model, and to ensure that the air passes over the model correctly. The balsa wood leading edge was made by gluing rectangular strips of balsa wood to the spars and filing down to shape, using the ribs as a guide, as shown in Figure 12.

FIGURE 12 WING MODEL WITH BALSA WOOD AEROFOIL SHAPED LEADING EDGE

3.1.3. Enabling Fixture of Model to Wind Tunnel

The model is attached to the wind tunnel via a plate interface shown in Figure 13. The plate is fixed to the wind tunnel by two screws but can be adjusted so that it is angled at certain degrees. Three blind holes were then drilled in the 'root' rib, one for a threaded rod and the remaining two were for locating pins. These pins were positioned forward and aft of the threaded rod, which was positioned in between the two inner spars. The pins located into the blind holes in the plate to ensure that the wing is always correctly fitted in the same position on the plate. By adjusting the angle of the plate, the wing's root angle of attack is also adjusted. Finally, the threaded rod fitted through the plate and wind tunnel and could then be bolted on to the wind tunnel wall.

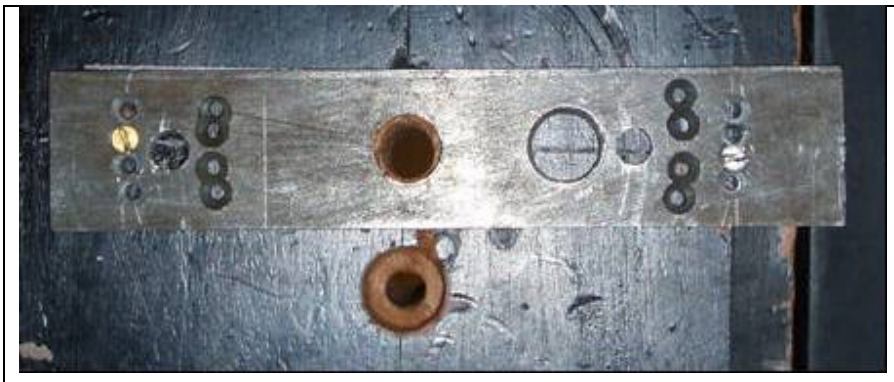

FIGURE 13. PLATE INTERFACE INCLINES AT 2º

3.1.4. Skinning of the Model

Once the model had been modified so that it was attachable to the wind tunnel, the ¾ wing was re-assembled and the connectors removed from the ¾ wing and device. Thin sheets of balsa wood were cut to tightly fit in between each rib at the trailing edge and were also held in place by glue. The purpose of these sheets was to prevent sticking of the solarfilm to itself from the top and bottom surfaces of the model, as this would not yield an acceptable aerofoil wing.

The device was then wrapped in solarfilm and an iron, with gradually increasing heat, was passed over the surfaces. As the solarfilm heated, it contracted and shrank to fit the shape of the device. The same procedure was followed for the ¾ wing, however, wrapping of this wing was much more difficult because the rod and pins were not removable. It was important to gradually increase the heat and ensure that the iron was not on the film for any length of time, or that the film would not overly stretch, otherwise damage to the film was likely to occur. This could result in ripping of the film and the process would have to be repeated. The completed wing with gust alleviation device is shown in Figure 14.

FIGURE 14 FINISHED WIND TUNNEL MODEL

Following the skinning of the model, it was then necessary to make small holes in the solarfilm at locations where the grub screw required accessing in order to fix or release the connector. Prior to making these holes tape was attached to the surface of the model at the relevant locations to prevent the holes made in the film from spreading.

4. WIND TUNNEL TESTS

4.1. Connector Stiffness

The wing and the gust device are connected by a cylinder which is fixed to both parts by grub screws. In order to get the desired stiffness the cylinder diameter is only 3mm and its length was 19mm. The material chosen was aluminium.

The stiffness can be calculated for a cylinder as:

$$Kf = \frac{G.J_T}{l} = \frac{G.d^4.p}{l \times 32}$$

G Aluminium = 80000 $\frac{N}{mm^2}$

Therefore for a cylinder of 0.019 m and 0.003m diameter we get

$$Kf = \frac{28 \times 10^9 \times 0.003^4 \times p}{0.019 \times 32} = 11.7 \text{ Nm/rad}$$

The problem with such a design is that the diameter enters the equation with the fourth power. The grub screws which fix the connector intrude in the cylinder and therefore reduce the diameter.

Assuming a diameter of 0.0015m to allow for the attachment we get 0.73 Nm/rad which is very close to the 1.05 Nm/rad which would give approximately 60% load alleviation due to the elastic twist.

4.2. Static Wind Tunnel Tests

The tests were performed with a root incidence of 3 degrees. In hindsight it might have been better to choose a larger value due to the presence of structural non-linearities that occur do to the small deflections that occurred. The wing was tested both with device operational and also a baseline case where the trailing edge was fixed to the wing, eliminating any effects of the gust alleviation device. Initially the wing was tested for varying tunnel speeds and static deflections measured.

In figure 15, deflections of rib 3 are plotted for the whole wing.

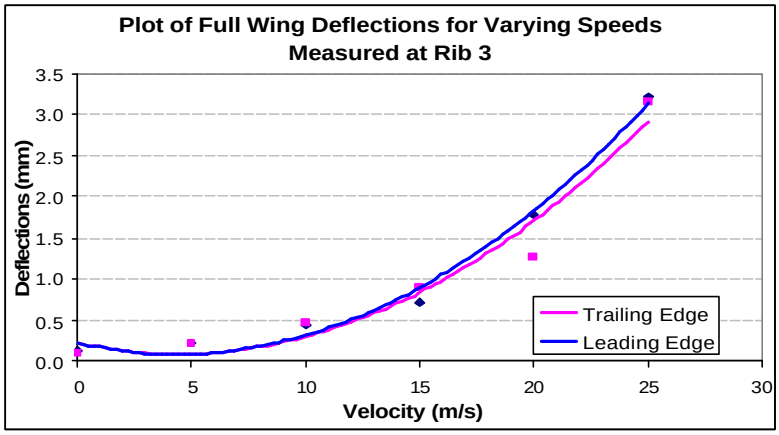

Figure 15. Full Wing Rib 3 deflections for varying speeds

Figure 16 shows deflections at rib 3 with the gust alleviation device working

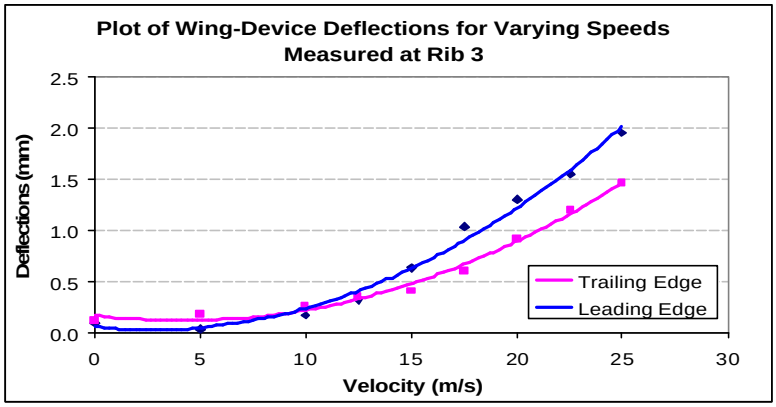

Figure 16. Wing with gust device Rib 3 deflections for varying speeds

In Table 2, the rib 3 trailing edge deflections are summarised. There are non-linearities present which mainly stem from fixing the connector to the wing (grub screws). Overall a reduction of deflection is shown when the gust device is used. For the highest speed the reduction in wing deflection is about 53% which correlates well with the theoretical calculations of the scaled 1:40 wind tunnel model.

	Full Wing	Wing Device	% Difference
0	0.1		
5	0.22		
10	0.46	0.27	42
15	0.88		
20	1.28	0.92	27
25	3.15	1.47	53

TABLE 2 RIB 3 TE DEFLECTIONS (mm) for Various Speeds

4.3. Dynamic Wind Tunnel Tests

A set of gust vanes were manufactured which are able to produce computer controlled vertical gusts into the tunnel – sinusoidal, “1-cosine” and random gusts can be produced. Figure 17 shows the gust vanes in the tunnel and the model.

Figure 17 Gust Vanes and the Model in the Wind Tunnel

Initial investigations concentrated upon the use of sinusoidal gust excitation, it was possible to tune the gust frequency in order to excite the first bending mode and to achieve significant deflections. Figures 18 and 19 shows the wing tip deflections with the gust device off and on. It can be seen that when the device is off, the leading and trailing edge deflections are very similar, indicating very little twist. With the on, the trailing edge deflects more than the leading edge, which shows that it works, and the deflections of the leading edge are less indicating that the bending motion is reduced.

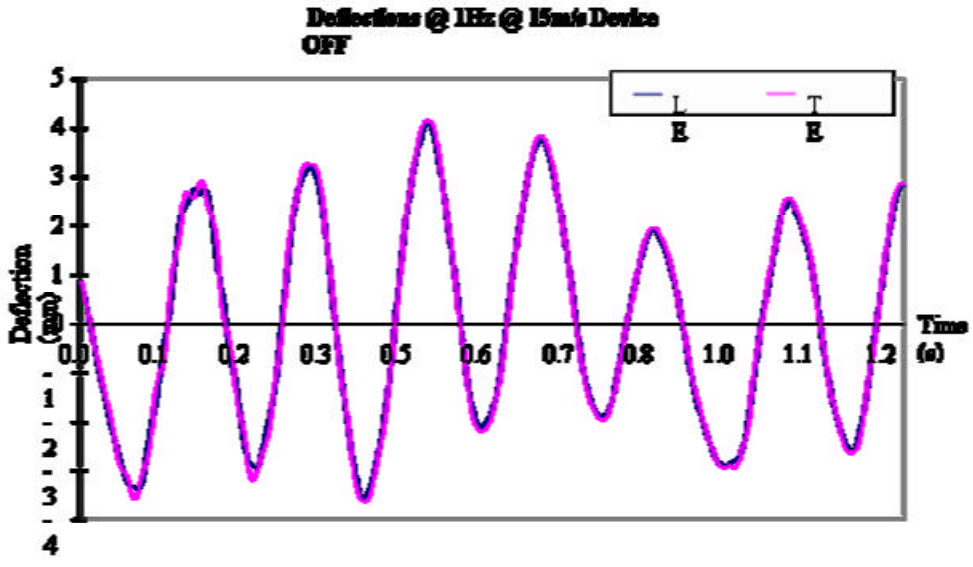

Figure 18. Leading and Trailing Edge Deflections Device Off

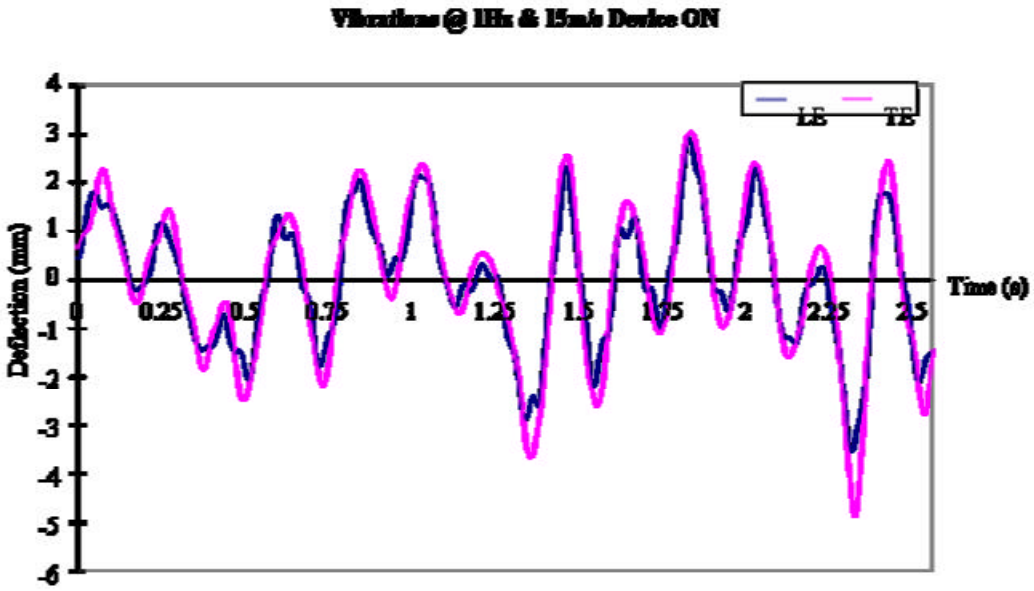

Figure 19. Leading and Trailing Edge Deflections Device On

5. Design of Wind Tunnel Sensorcraft Model

The next part of this work involves the design, manufacture and testing of a larger half Sensorcraft model to be tested in the 9'x7' tunnel at the University of Manchester. This was initially going to take the form of a 1:20 model however following discussions with Dr Max Blair and co-workers the baseline structure has changed, and will now follow the Boeing design shown in Figure 20. The gust alleviation device will be incorporated into the structure, and in the same way as the prototype wing discussed above, tests will be performed with and without the device being activated.

It is planned that a PhD student from AFIT will spend some time in Manchester assisting with the tests, also investigating the non-linear geometric behaviour at high static loading cases.

There were a number of difficulties in actually defining the parameters of the model (we were not allowed to have access to the FE model) and consequently only some initial analysis has been performed.

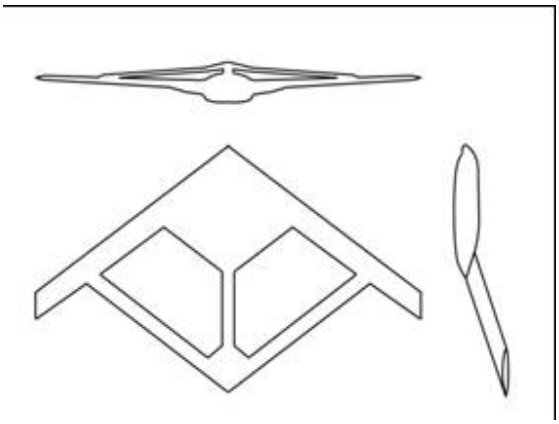

Figure 20. Baseline Structure for Future Work

6. Aeroelastic Scaling

6.1. Objectives

- To define a **dynamically** scaled aeroelastic model that responds identically to a full-scale design with respect to chosen scale factors (e.g. geometric scaling, velocity scaling etc). This goal can be achieved on the basis of a set of non-dimensional aeroelastic equations.
- To eliminate the reliance of the BAH [3] scaling approach on equivalent beams

6.2. Approach

- Based on wind-tunnel parameters, identify maximum geometry scale and maximum velocity scale. For a dynamically scaled test, will also need to identify a third scale (e.g. mass);
- Identify the governing non-dimensional equations of motion (EOM) that will be numerically identical for both the scaled and full-scale designs. The choice of degrees of freedom must serve both models. The common degrees of freedom may be reflected on a global scale with modal coordinates or a local scale with influence coefficients interpolated at common points.
- Start the scaled model design process by defining the flexible structure. This layout could be a lattice of beams (but not necessarily – could be ribs and spars. or perhaps an equivalent plate).
- Size the scaled model structure according to the scaling parameters. This step depends on the form of the governing aeroelastic equations of motion.

6.3. Non-Dimensionalised Aeroelastic Equations of Motion

In order to achieve a non-dimensional set of equations, we need to select 3 base units of measurement for dynamic analysis, typically mass, length and velocity (length / time) although force, length and velocity

could also be chosen. For static analysis we only need 2 base units of measurement - force and length (the time dependent term is removed).

The following equations assume we have reduced the equations of motion to a minimum of two degrees of freedom that represent displacement (length) and rotation (non-dimensional). These two degrees of freedom are consistent with most commercial finite element codes.

Taking a coupled FE / Aerodynamic equations of motion (ignoring structural damping) such that

$$\begin{bmatrix} \mathbf{M}_{11} & \mathbf{M}_{12} \\ \mathbf{M}_{21} & \mathbf{M}_{22} \end{bmatrix} \begin{Bmatrix} \ddot{\mathbf{X}} \\ \ddot{q} \end{Bmatrix} + \begin{bmatrix} \mathbf{K}_{11} & \mathbf{K}_{12} \\ \mathbf{K}_{21} & \mathbf{K}_{22} \end{bmatrix} \begin{Bmatrix} \mathbf{X} \\ q \end{Bmatrix} = \frac{\rho \mathbf{V}^2}{2} \begin{bmatrix} \mathbf{b}^2 & 0 \\ 0 & \mathbf{b}^3 \end{bmatrix} \begin{bmatrix} \mathbf{Q}_{11} & \mathbf{Q}_{12} \\ \mathbf{Q}_{21} & \mathbf{Q}_{22} \end{bmatrix} \begin{Bmatrix} \mathbf{X} \\ q \end{Bmatrix} \qquad (1)$$

where

$\mathbf{X}$	Vector of translational degrees of freedom
q	Vector of rotational degrees of freedom
$\mathbf{M}_{ij}$	Block matrix terms in inertia / mass matrix
$\mathbf{K}_{ij}$	Block matrix terms in stiffness matrix
$\mathbf{b}$	Reference length (semi-chord)
$\mathbf{Q}_{ij}$	Block matrix Aerodynamic terms (complex for unsteady motions)

In terms of dimensions of the fundamental quantities (M, L, T) equation (1) has the form

$$\begin{bmatrix} \mathbf{M} & \mathbf{ML} \\ \mathbf{ML} & \mathbf{ML}^2 \end{bmatrix} \begin{Bmatrix} \mathbf{LT}^{-2} \\ \mathbf{T}^{-2} \end{Bmatrix} + \begin{bmatrix} \mathbf{MT}^{-2} & \mathbf{MLT}^{-2} \\ \mathbf{MLT}^{-2} & \mathbf{ML}^2\mathbf{T}^{-2} \end{bmatrix} \begin{Bmatrix} \mathbf{L} \\ \mathbf{ND} \end{Bmatrix} = \mathbf{ML}^{-1}\mathbf{T}^{-2} \begin{bmatrix} \mathbf{L}^2 & 0 \\ 0 & \mathbf{L}^3 \end{bmatrix} \begin{bmatrix} \mathbf{L}^{-1} & \mathbf{ND} \\ \mathbf{L}^{-1} & \mathbf{ND} \end{bmatrix} \begin{Bmatrix} \mathbf{L} \\ \mathbf{ND} \end{Bmatrix} \qquad (2)$$

Thus, according to Newtonian mechanics, we have three base scaling parameters of mass, length and time.

6.4. Base Scaling Parameters

Geometric Scaling: Defining the non-dimensional coordinate system (x, f) such that

$$\mathbf{x} = \mathbf{b}x \qquad \textbf{and} \qquad q = f \qquad (3)$$

Time Scaling: non-dimensional time $t = \frac{\mathbf{V}t}{\mathbf{b}}$. Thus, the base time unit is indirectly scaled in terms of a (surrogate) velocity and geometric scale – which reflects the requirement that the scaled model operate within the wind tunnel operational limits. Use the chain rule to non-dimensionalize time derivatives that are present in the governing equations of motion.

$$\dot{\mathbf{x}} = \mathbf{V}x' \quad \ddot{\mathbf{x}} = \frac{\mathbf{V}^2}{\mathbf{b}}x'' \qquad \dot{q} = \frac{\mathbf{V}}{\mathbf{b}}f' \qquad \ddot{q} = \frac{\mathbf{V}^2}{\mathbf{b}^2}f'' \tag{4}$$

where (.) denotes differentiation w.r.t time and (‘) denotes differentiation w.r.t non-dimensional time.

Mass Scaling: There are a number of options for scaling the mass. These are discussed below. Mass can be scaled directly (e.g. total mass of the airplane). Mass can also be scaled in terms of a surrogate density scale. Also, since Force is mass times acceleration, units of force can be used as a derivative (or surrogate) scaling parameter for mass.

Equation (2) will be rendered non-dimensional according to the three scaling parameters.

6.5. Mass Scaling

The first approach will consider using some reference mass $\mathbf{m}_r$ as part of the scaling process.

Non-Dimensionalised Inertial Force

Defining non-dimensional inertia terms (denoted by the overbar)

$$\mathbf{M}_{11} = \mathbf{m}_r\bar{\mathbf{M}}_{11} \qquad \mathbf{M}_{12} = \mathbf{m}_r\mathbf{b}\bar{\mathbf{M}}_{12} \qquad \mathbf{M}_{21} = \mathbf{m}_r\mathbf{b}\bar{\mathbf{M}}_{21} \qquad \mathbf{M}_{22} = \mathbf{m}_r\mathbf{b}^2\bar{\mathbf{M}}_{22} \tag{5}$$

where $\mathbf{m}_r$ is some reference mass (e.g. total mass of the full structure) then the force and moment resulting from the mass and inertial terms can be written as

$$\begin{Bmatrix} \mathbf{F} \\ \mathbf{M}_P \end{Bmatrix} = \begin{bmatrix} \mathbf{M}_{11} & \mathbf{M}_{12} \\ \mathbf{M}_{21} & \mathbf{M}_{22} \end{bmatrix} \begin{Bmatrix} \ddot{\mathbf{x}} \\ \dot{q}_P \end{Bmatrix} = \begin{bmatrix} \mathbf{m}_r\bar{\mathbf{M}}_{11} & \mathbf{m}_r\mathbf{b}\bar{\mathbf{M}}_{12} \\ \mathbf{m}_r\mathbf{b}\bar{\mathbf{M}}_{21} & \mathbf{m}_r\mathbf{b}^2\bar{\mathbf{M}}_{22} \end{bmatrix} \begin{Bmatrix} \frac{\mathbf{V}^2}{\mathbf{b}}x'' \\ \frac{\mathbf{V}^2}{\mathbf{b}^2}f''_P \end{Bmatrix} \tag{6}$$

thus

$$\begin{Bmatrix}\mathbf{F}\\ \mathbf{M}_I\end{Bmatrix} = \begin{bmatrix}\frac{\mathbf{m_r V^2}}{\mathbf{b}}\bar{\mathbf{M}}_{11} & \frac{\mathbf{m_r V^2}}{\mathbf{b}}\bar{\mathbf{M}}_{12}\\ \mathbf{m_r V^2}\bar{\mathbf{M}}_{21} & \mathbf{m_r V^2}\bar{\mathbf{M}}_{22}\end{bmatrix}\begin{Bmatrix}x\\ \theta\end{Bmatrix} = \begin{bmatrix}\frac{\mathbf{m_r V^2}}{\mathbf{b}} & 0\\ 0 & \mathbf{m_r V^2}\end{bmatrix}\begin{bmatrix}\bar{\mathbf{M}}_{11} & \bar{\mathbf{M}}_{12}\\ \bar{\mathbf{M}}_{21} & \bar{\mathbf{M}}_{22}\end{bmatrix}\begin{Bmatrix}x\\ \theta\end{Bmatrix} \tag{7}$$

$$= \begin{bmatrix}\frac{\mathbf{m_r V^2}}{\mathbf{b}} & 0\\ 0 & \mathbf{m_r V^2}\end{bmatrix}\begin{Bmatrix}\bar{\mathbf{F}}\\ \bar{\mathbf{M}}\end{Bmatrix}_I$$

where $\bar{\mathbf{F}}$ and $\bar{\mathbf{M}}$ are non-dimensional forces and moments respectively.

Non-Dimensionalised Stiffness Force

The process for the stiffness terms follows the same procedure as that shown above for the inertia terms. Defining

$$\mathbf{K}_{11} = \frac{\mathbf{m_r V^2}}{\mathbf{b^2}}\bar{\mathbf{K}}_{11} \qquad \mathbf{K}_{12} = \frac{\mathbf{m_r V^2}}{\mathbf{b}}\bar{\mathbf{K}}_{12} \qquad \mathbf{K}_{21} = \frac{\mathbf{m_r V^2}}{\mathbf{b}}\bar{\mathbf{K}}_{21} \qquad \mathbf{K}_{22} = \mathbf{m_r V^2}\bar{\mathbf{K}}_{22} \tag{8}$$

then the force and moment resulting from the stiffness terms can be written as

$$\begin{Bmatrix}\mathbf{F}\\ \mathbf{M}\end{Bmatrix}_S = \begin{bmatrix}\mathbf{K}_{11} & \mathbf{K}_{12}\\ \mathbf{K}_{21} & \mathbf{K}_{22}\end{bmatrix}\begin{Bmatrix}\mathbf{x}\\ \theta\end{Bmatrix} = \begin{bmatrix}\frac{\mathbf{m_r V^2}}{\mathbf{b^2}}\bar{\mathbf{K}}_{11} & \frac{\mathbf{m_r V^2}}{\mathbf{b}}\bar{\mathbf{K}}_{12}\\ \frac{\mathbf{m_r V^2}}{\mathbf{b}}\bar{\mathbf{K}}_{21} & \mathbf{m_r V^2}\bar{\mathbf{K}}_{22}\end{bmatrix}\begin{Bmatrix}\mathbf{b}x\\ f\end{Bmatrix} \tag{9}$$

thus

$$\begin{Bmatrix}\mathbf{F}\\ \mathbf{M}\end{Bmatrix}_S = \begin{bmatrix}\frac{\mathbf{m_r V^2}}{\mathbf{b}}\bar{\mathbf{K}}_{11} & \frac{\mathbf{m_r V^2}}{\mathbf{b}}\bar{\mathbf{K}}_{12}\\ \mathbf{m_r V^2}\bar{\mathbf{K}}_{21} & \mathbf{m_r V^2}\bar{\mathbf{K}}_{22}\end{bmatrix}\begin{Bmatrix}x\\ f\end{Bmatrix} = \begin{bmatrix}\frac{\mathbf{m_r V^2}}{\mathbf{b}} & 0\\ 0 & \mathbf{m_r V^2}\end{bmatrix}\begin{bmatrix}\bar{\mathbf{K}}_{11} & \bar{\mathbf{K}}_{12}\\ \bar{\mathbf{K}}_{21} & \bar{\mathbf{K}}_{22}\end{bmatrix}\begin{Bmatrix}x\\ f\end{Bmatrix} \tag{10}$$

$$= \begin{bmatrix}\frac{\mathbf{m_r V^2}}{\mathbf{b}} & 0\\ 0 & \mathbf{m_r V^2}\end{bmatrix}\begin{Bmatrix}\bar{\mathbf{F}}\\ \bar{\mathbf{M}}\end{Bmatrix}_S$$

Non-Dimensionalised Aeroelastic Equations

Introducing transformations (3) and (4) into equation (1) and pre-multiplying by

$$Y = \begin{bmatrix} \frac{\mathbf{b}}{\mathbf{m_r V}^2} & 0 \\ 0 & \frac{1}{\mathbf{m_r V}^2} \end{bmatrix} \tag{11}$$

gives the redefined system equations as

$$\begin{bmatrix} \bar{\mathbf{M}}_{11} & \bar{\mathbf{M}}_{12} \\ \bar{\mathbf{M}}_{21} & \bar{\mathbf{M}}_{22} \end{bmatrix} \begin{Bmatrix} \ddot{x} \\ \ddot{\theta} \end{Bmatrix} + \begin{bmatrix} \bar{\mathbf{K}}_{11} & \bar{\mathbf{K}}_{12} \\ \bar{\mathbf{K}}_{21} & \bar{\mathbf{K}}_{22} \end{bmatrix} \begin{Bmatrix} x \\ \theta \end{Bmatrix} = \begin{bmatrix} \frac{\rho \mathbf{b}^3}{2\mathbf{m_r}} & 0 \\ 0 & \frac{\rho \mathbf{b}^3}{2\mathbf{m_r}} \end{bmatrix} \begin{bmatrix} \mathbf{b}\mathbf{Q}_{11} & \mathbf{Q}_{12} \\ \mathbf{b}\mathbf{Q}_{21} & \mathbf{Q}_{22} \end{bmatrix} \begin{Bmatrix} x \\ \theta \end{Bmatrix} \tag{12}$$

Note that the Q matrix now becomes fully non-dimensional.

6.6. Density Scaling

A second approach will consider using the air density as part of the scaling process

Non-Dimensionalised Inertial Force

Defining non-dimensional inertia terms (denoted by the overbar)

$$\mathbf{M}_{11} = \rho \mathbf{b}^3 \bar{\mathbf{M}}_{11} \qquad \mathbf{M}_{12} = \rho \mathbf{b}^4 \bar{\mathbf{M}}_{12} \qquad \mathbf{M}_{21} = \rho \mathbf{b}^4 \bar{\mathbf{M}}_{21} \qquad \mathbf{M}_{22} = \rho \mathbf{b}^5 \bar{\mathbf{M}}_{22} \tag{13}$$

where ρ is the air density and $\mathbf{b}$ is some defined length, then the force and moment resulting from the mass and inertial terms can be written as

$$\begin{Bmatrix} \mathbf{F} \\ \mathbf{M}_{\mathbf{I}} \end{Bmatrix} = \begin{bmatrix} \mathbf{M}_{11} & \mathbf{M}_{12} \\ \mathbf{M}_{21} & \mathbf{M}_{22} \end{bmatrix} \begin{Bmatrix} \ddot{\mathbf{x}} \\ \ddot{\theta} \end{Bmatrix} = \begin{bmatrix} \rho \mathbf{b}^3 \bar{\mathbf{M}}_{11} & \rho \mathbf{b}^4 \bar{\mathbf{M}}_{12} \\ \rho \mathbf{b}^4 \bar{\mathbf{M}}_{21} & \rho \mathbf{b}^5 \bar{\mathbf{M}}_{22} \end{bmatrix} \begin{Bmatrix} \frac{\mathbf{V}^2}{\mathbf{b}} \ddot{x} \\ \frac{\mathbf{V}^2}{\mathbf{b}^2} \ddot{\theta} \end{Bmatrix} \tag{14}$$

thus

$$\begin{Bmatrix}\mathbf{F}\\ \mathbf{M}\end{Bmatrix}_{\mathrm{I}} = \begin{bmatrix}\rho\mathbf{V}^2\mathbf{b}^2\bar{\mathbf{M}}_{11} & \rho\mathbf{V}^2\mathbf{b}^2\bar{\mathbf{M}}_{12}\\ \rho\mathbf{V}^2\mathbf{b}^3\bar{\mathbf{M}}_{21} & \rho\mathbf{V}^2\mathbf{b}^3\bar{\mathbf{M}}_{22}\end{bmatrix}\begin{Bmatrix}\ddot{x}\\ \ddot{\theta}\end{Bmatrix} = \begin{bmatrix}\rho\mathbf{V}^2\mathbf{b}^2 & 0\\ 0 & \rho\mathbf{V}^2\mathbf{b}^3\end{bmatrix}\begin{bmatrix}\bar{\mathbf{M}}_{11} & \bar{\mathbf{M}}_{12}\\ \bar{\mathbf{M}}_{21} & \bar{\mathbf{M}}_{22}\end{bmatrix}\begin{Bmatrix}\ddot{x}\\ \ddot{\theta}\end{Bmatrix} = \begin{bmatrix}\rho\mathbf{V}^2\mathbf{b}^2 & 0\\ 0 & \rho\mathbf{V}^2\mathbf{b}^3\end{bmatrix}\begin{Bmatrix}\bar{\mathbf{F}}\\ \bar{\mathbf{M}}\end{Bmatrix}_{\mathrm{I}} \quad (15)$$

where $\bar{\mathbf{F}}$ and $\bar{\mathbf{M}}$ are non-dimensional forces and moments respectively.

Non-Dimensionalised Stiffness Force

The process for the stiffness terms follows the same procedure as that shown above for the inertia terms. Defining

$$\mathbf{K}_{11} = \rho\mathbf{b}\mathbf{V}^2\bar{\mathbf{K}}_{11} \qquad \mathbf{K}_{12} = \rho\mathbf{b}^2\mathbf{V}^2\bar{\mathbf{K}}_{12} \qquad \mathbf{K}_{21} = \rho\mathbf{b}^2\mathbf{V}^2\bar{\mathbf{K}}_{21} \qquad \mathbf{K}_{22} = \rho\mathbf{b}^3\mathbf{V}^2\bar{\mathbf{K}}_{22} \quad (16)$$

then the force and moment resulting from the stiffness terms can be written as

$$\begin{Bmatrix}\mathbf{F}\\ \mathbf{M}\end{Bmatrix}_{\mathrm{S}} = \begin{bmatrix}\mathbf{K}_{11} & \mathbf{K}_{12}\\ \mathbf{K}_{21} & \mathbf{K}_{22}\end{bmatrix}\begin{Bmatrix}\mathbf{x}\\ \theta\end{Bmatrix} = \begin{bmatrix}\rho\mathbf{b}\mathbf{V}^2\bar{\mathbf{K}}_{11} & \rho\mathbf{b}^2\mathbf{V}^2\bar{\mathbf{K}}_{12}\\ \rho\mathbf{b}^2\mathbf{V}^2\bar{\mathbf{K}}_{21} & \rho\mathbf{b}^3\mathbf{V}^2\bar{\mathbf{K}}_{22}\end{bmatrix}\begin{Bmatrix}\mathbf{b}x\\ \theta\end{Bmatrix} \quad (17)$$

thus

$$\begin{Bmatrix}\mathbf{F}\\ \mathbf{M}\end{Bmatrix}_{\mathrm{S}} = \begin{bmatrix}\rho\mathbf{b}^2\mathbf{V}^2\bar{\mathbf{K}}_{11} & \rho\mathbf{b}^2\mathbf{V}^2\bar{\mathbf{K}}_{12}\\ \rho\mathbf{b}^3\mathbf{V}^2\bar{\mathbf{K}}_{21} & \rho\mathbf{b}^3\mathbf{V}^2\bar{\mathbf{K}}_{22}\end{bmatrix}\begin{Bmatrix}x\\ \theta\end{Bmatrix} = \begin{bmatrix}\rho\mathbf{b}^2\mathbf{V}^2 & 0\\ 0 & \rho\mathbf{b}^3\mathbf{V}^2\end{bmatrix}\begin{bmatrix}\bar{\mathbf{K}}_{11} & \bar{\mathbf{K}}_{12}\\ \bar{\mathbf{K}}_{21} & \bar{\mathbf{K}}_{22}\end{bmatrix}\begin{Bmatrix}x\\ \theta\end{Bmatrix} = \begin{bmatrix}\rho\mathbf{b}^2\mathbf{V}^2 & 0\\ 0 & \rho\mathbf{b}^3\mathbf{V}^2\end{bmatrix}\begin{Bmatrix}\bar{\mathbf{F}}\\ \bar{\mathbf{M}}\end{Bmatrix}_{\mathrm{S}} \quad (18)$$

Non-Dimensionalised Aeroelastic Equations

Introducing transformations (13) and (16) and pre-multiplying equation (1) by

$$\mathrm{Y} = \begin{bmatrix}\dfrac{1}{\rho\mathbf{b}^2\mathbf{V}^2} & 0\\ 0 & \dfrac{1}{\rho\mathbf{b}^3\mathbf{V}^2}\end{bmatrix} \quad (19)$$

gives the redefined system equations as

$$\begin{bmatrix} \bar{\mathbf{M}}_{11} & \bar{\mathbf{M}}_{12} \\ \bar{\mathbf{M}}_{21} & \bar{\mathbf{M}}_{22} \end{bmatrix} \begin{Bmatrix} \ddot{x} \\ \ddot{f} \end{Bmatrix} + \begin{bmatrix} \bar{\mathbf{K}}_{11} & \bar{\mathbf{K}}_{12} \\ \bar{\mathbf{K}}_{21} & \bar{\mathbf{K}}_{22} \end{bmatrix} \begin{Bmatrix} x \\ f \end{Bmatrix} = \begin{bmatrix} 1/2 & 0 \\ 0 & 1/2 \end{bmatrix} \begin{bmatrix} \mathbf{bQ}_{11} & \mathbf{Q}_{12} \\ \mathbf{bQ}_{21} & \mathbf{Q}_{22} \end{bmatrix} \begin{Bmatrix} x \\ f \end{Bmatrix} \qquad (20)$$

Again, the Q matrix now becomes fully non-dimensional. It is arguable that this is a better form to use as there is only a length scaling that needs to be changed, however, there are now no longer any density or mass terms directly visible in equation (20).

6.7. Scaling of the Aeroelastic Equations

We have arrived at two different non-dimensional sets of aeroelastic equations (12) and (20). These equations can be used to determine the system behaviour for any combination of fundamental quantities $\mathbf{r,b,m_r}$ or $\mathbf{r,b,V}$ respectively using the scaling relationships (5) and (8) or (13) and (16) respectively. If the full size and model structure (physical construction and FE / aerodynamic models) are exactly the same, then these scaling relationships determine the scaled model characteristics.

However, in practice the model structure is not constructed in the same way as the full size aircraft, and the finite element and aerodynamic models will also not be the same therefore the above scaling relationships can be used to provide “target” characteristics for the scaled model. For the rest of this section the mass scaling approach will be used but the density scaling approach, or any other, could be used as well.

Wind-Off Natural Frequencies and Mode Shapes

The natural frequencies and corresponding mode shapes of the full scale system are obtained from the eigensolution of the matrix

$$\mathbf{D}\,\mathrm{F} = \mathrm{F}\,\mathrm{W} \qquad (21)$$

where

$$\mathbf{D} = \begin{bmatrix} \mathbf{M}_{11} & \mathbf{M}_{12} \end{bmatrix}^{-1} \begin{bmatrix} \mathbf{K}_{11} & \mathbf{K}_{12} \\ \mathbf{M}_{21} & \mathbf{M}_{22} \end{bmatrix}$$

$$W = \mathbf{diag}\left[w_1^2, w_2^2, \ldots w_N^2 \right] \quad (\mathbf{eigenvalues}) \tag{22}$$

$$F = \left[\{f_1\}, \{f_2\}, \ldots \{f_N\} \right] \quad \mathbf{(eigenvectors = modeshapes)}$$

and the natural frequencies have units of rad s^{-1} whereas the mode shapes are non-dimensional.

In terms of the non-dimensionalised equations of motion (taking the mass scaling route), the natural frequencies and corresponding mode shapes are obtained from the eigensolution of the matrix

$$\bar{\mathbf{D}}\bar{F} = \bar{F}\bar{W} \tag{23}$$

where

$$\bar{\mathbf{D}} = \begin{bmatrix} \bar{\mathbf{M}}_{11} & \bar{\mathbf{M}}_{12} \end{bmatrix}^{-1} \begin{bmatrix} \bar{\mathbf{K}}_{11} & \bar{\mathbf{K}}_{12} \\ \bar{\mathbf{M}}_{21} & \bar{\mathbf{M}}_{22} \end{bmatrix}$$

$$\bar{W} = \mathbf{diag}\left[\bar{w}_1^2, \bar{w}_2^2, \ldots \bar{w}_N^2 \right] \quad (\mathbf{eigenvalues}) \tag{24}$$

$$\bar{F} = \left[\{f_1\}, \{f_2\}, \ldots \{f_N\} \right] = F \quad \mathbf{(eigenvectors = modeshapes)}$$

and the natural frequencies now have units of rad τ^{-1}. Unfortunately at zero airspeed the scaling has no meaning and therefore the dynamic analysis must be performed with the inclusion of the velocity dependent aerodynamic terms.

Wind-on Natural Frequencies and Mode Shapes

Considering the system when there is some airspeed, the non-dimensionalised frequencies, dampings and mode shapes are found from the solution of equation (25).

$$\begin{bmatrix} \bar{\mathbf{M}}_{11} & \bar{\mathbf{M}}_{12} \\ \bar{\mathbf{M}}_{21} & \bar{\mathbf{M}}_{22} \end{bmatrix} \begin{Bmatrix} \ddot{x} \\ \ddot{f} \end{Bmatrix} + \left(\begin{bmatrix} \bar{\mathbf{K}}_{11} & \bar{\mathbf{K}}_{12} \\ \bar{\mathbf{K}}_{21} & \bar{\mathbf{K}}_{22} \end{bmatrix} - \begin{bmatrix} \frac{\rho \mathbf{b}^3}{2\mathbf{m}_r} & 0 \\ 0 & \frac{\rho \mathbf{b}^3}{2\mathbf{m}_r} \end{bmatrix} \begin{bmatrix} \mathbf{bQ}_{11} & \mathbf{Q}_{12} \\ \mathbf{bQ}_{21} & \mathbf{Q}_{22} \end{bmatrix} \right) \begin{Bmatrix} x \\ f \end{Bmatrix} = \begin{Bmatrix} 0 \\ 0 \end{Bmatrix} \tag{25}$$

Although the structural terms remain the same whatever the scaling, the aerodynamic terms do change depending upon the triple (m, ?, b). Remember that the frequencies that are obtained are in non-dimensional time and thus are scaled by $\mathbf{b}/\mathbf{V}$ and that the mode shapes are complex.

Static Aeroelastic Deflections

The static aeroelastic deflections depend upon there being some initial incidence on some parts of the lifting surfaces. In terms of the non-dimensionalised equations (25) we get

$$\left(\begin{bmatrix}\bar{\mathbf{K}}_{11} & \bar{\mathbf{K}}_{12}\\ \bar{\mathbf{K}}_{21} & \bar{\mathbf{K}}_{22}\end{bmatrix} - \begin{bmatrix}\frac{\rho \mathbf{b}^3}{2\mathbf{m}_r} & 0\\ 0 & \frac{\rho \mathbf{b}^3}{2\mathbf{m}_r}\end{bmatrix}\begin{bmatrix}\mathbf{bQ}_{11} & \mathbf{Q}_{12}\\ \mathbf{bQ}_{21} & \mathbf{Q}_{22}\end{bmatrix}\right)\begin{Bmatrix}\xi\\ \phi\end{Bmatrix} = \begin{bmatrix}\frac{\rho \mathbf{b}^3}{2\mathbf{m}_r} & 0\\ 0 & \frac{\rho \mathbf{b}^3}{2\mathbf{m}_r}\end{bmatrix}\begin{bmatrix}\mathbf{bQ}_{11} & \mathbf{Q}_{12}\\ \mathbf{bQ}_{21} & \mathbf{Q}_{22}\end{bmatrix}\begin{Bmatrix}0\\ \phi_0\end{Bmatrix} \quad (26)$$

where ϕ_0 are a set of initial angles of incidence. The deflections ξ, ϕ that are found are non-dimensionalised.

6.8. Practical Application of Aeroelastic Scaling

In practice, the problem is defined as to find an equivalent aeroelastically scaled model structure given the FE and aerodynamic models of a full scale structure at specified flight conditions. Although the geometric scaling holds for the planform of the model, the internal structure is likely to be different, possibly not even made of the same material or construction technique; similarly, the FE and aerodynamic models corresponding to the scaled structure will also be different. The wind tunnel chosen to perform the tests will constrain the dimensions of the model and the speed it is tested at.

The differences between the full scale (subscript s) and model (subscript m - physical and computational) mean that it is not possible to simply scale the FE matrices. Instead comparison must be made of quantities such as modal quantities (frequencies and mode shapes), influence coefficients and non-dimensionalised deflections.

Here it is proposed to use the following scaled quantities.

1. Geometric Scaling

$$\mathbf{L}_s = \mathbf{n}_g \mathbf{L}_m \quad (27)$$

2. Velocity Scaling

$$\mathbf{V_s} = \mathbf{n_v V_m} \tag{28}$$

3. Air Density Scaling

$$\rho_s = \mathbf{n}_\rho \rho_m \tag{29}$$

Note that the Equivalent Air Speed could be used in order to eliminate the need for density information.

4. Natural Frequencies

Rewriting the aeroelastic equations in non-dimensional form involves the transformation into non-dimensional time. The natural frequencies of the full-scale and model structure at the reference test conditions must be the same, thus

$$\frac{\omega_s \mathbf{b_s}}{\mathbf{V_s}} = \frac{\omega_m \mathbf{b_m}}{\mathbf{V_m}} \quad \Rightarrow \quad \omega_m = \frac{\mathbf{V_m}}{\mathbf{V_s}} \frac{\mathbf{b_s}}{\mathbf{b_m}} \omega_s = \frac{\mathbf{n_s}}{\mathbf{n_v}} \omega_s \tag{30}$$

i.e. the reduced frequencies must remain the same.

5. Mode Shapes

The mode shapes corresponding to the various natural frequencies of the full scale and model structure must be the same. These shapes will be complex to some degree depending upon the characteristics of the unsteady aerodynamics terms.

6. Static Aeroelastic Deflections

The non-dimensionalised static aeroelastic equations (26) show that equivalent non-dimensionalised deflections at the reference test conditions must be the same. e.g. for the wing tip at the reference conditions

$$\left(\frac{x_{tip}}{b} \right)_s = \left(\frac{x_{tip}}{b} \right)_m \tag{31}$$

7. Gust Response

Gust velocities will scale in the same way as the airspeed. In order to achieve an equivalent scaled response, the same maximum normalised deflection at some points of the structure to the scaled gust must be obtained.

$$\left(V_{gust}\right)_s = n_v \left(V_{gust}\right)_m \qquad \left(\frac{xmax_{tip}}{b}\right)_s = \left(\frac{x\,max_{tip}}{b}\right)_m \tag{32}$$

8. Non-Linear Static Aeroelastic Deflections

Although the FE model of a non-linear analysis is much more complicated than the linear description shown above, a similar scaling approach can be used. In the same way as for the linear static aeroelastic deflections, the equivalent non-dimensionalised non-linear deflections at the reference test conditions must be the same. e.g. for the wing tip at the reference conditions

$$\left(\frac{x_{tip}}{b}\right)_s = \left(\frac{x_{tip}}{b}\right)_m \tag{33}$$

and this will enable any non-linear deflection behaviour to be scaled.

9. Buckling

The critical speed at which buckling (linear or non-linear) will occur simply depends upon the velocity scaling

$$\left(V_{buckling}\right)_s = n_v \left(V_{buckling}\right)_m \tag{34}$$

Given the above geometric, velocity and density scalings, an aeroelastically scaled FE model can be found by optimising the dimensions of the internal structure and skin thickness (and possible extra distributed masses) to meet a series of pre-defined reduced frequencies, mode shapes, non-dimensionalised static aeroelastic deflections and, if required, gust and buckling behaviour. It is unlikely that an exact match will be made for all conditions.

7. Example of Optimisation Approach

The optimisation approach was developed using a NASTRAN finite-element model of a Convair 990 (see figure 21). The objective was to create a 2-spar and multi-ribbed wing that would have similar (within 5-

10% for the first few modes) modal properties to the original aircraft wing, whilst not altering the geometric plan-form properties of the aircraft.

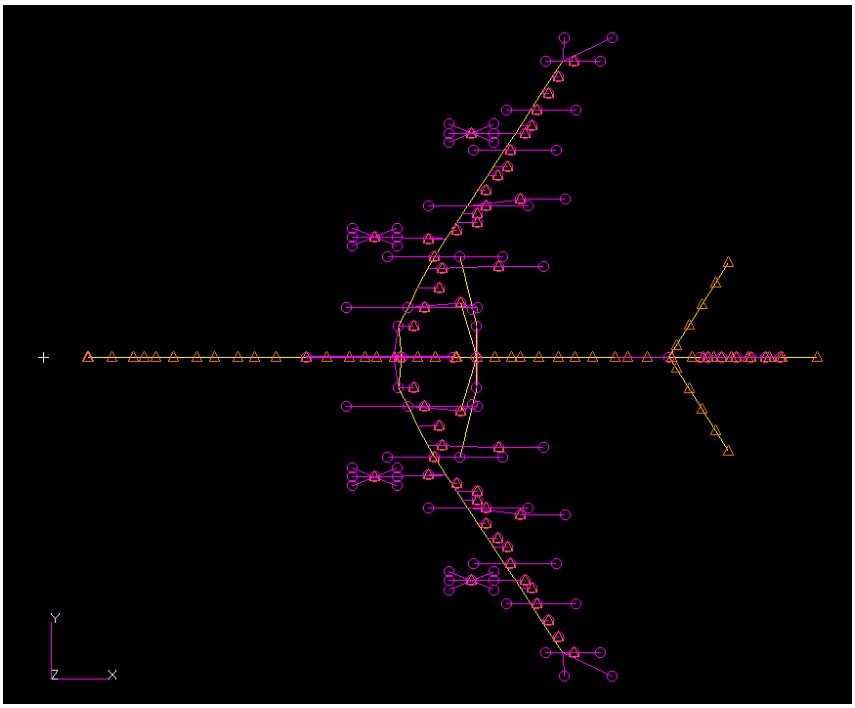

Figure 21. Aircraft FE Model

7.1. Method

The original Convair 990 FE wing (see figure 22) is a representation of the true wing, with the PBEAM elements (yellow, running from root to tip forming a single line) having no physical, inertial or stiffness resemblance to the true spar. The first step was to reduce the FE model down to the starboard wing so that the mode shapes could easily be identified. Next, a modal analysis of this wing was performed, the resulting modes being those that were to be re-created in the modified model. The original spanwise beam was then removed and two new spanwise beams were added at quarter and three-quarter chord positions to represent the two spars. Additionally, 6 beams were added to model the ribs (see figure 23). A MATLAB program was then written to allow Genetic Algorithm (G.A.) optimisation via a macro program with NASTRAN. Each spar was divided into 4 property sets and each rib formed a property set resulting in 14 property sets. The mass and stiffness properties of each spar element and rib element (both rectangular cross-sections) were controlled via the variation of the cross-sectional dimensions (width and depth), giving a total of 28 variables in the model. These variables were restricted within a specified range in order to allow any solution to be realistic. The G.A. program creates an initial set of these variables, then NASTRAN runs the analysis with these values. The G.A. program then compares the new modal

frequencies to the target frequencies before creating a new set of variables biased towards a better solution. This process continues until suitable convergence is achieved.

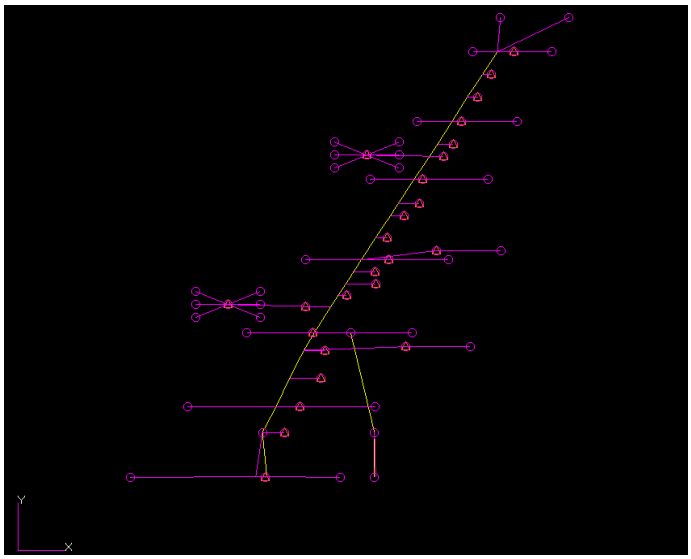

Figure 22. Aircraft Wing FE Model

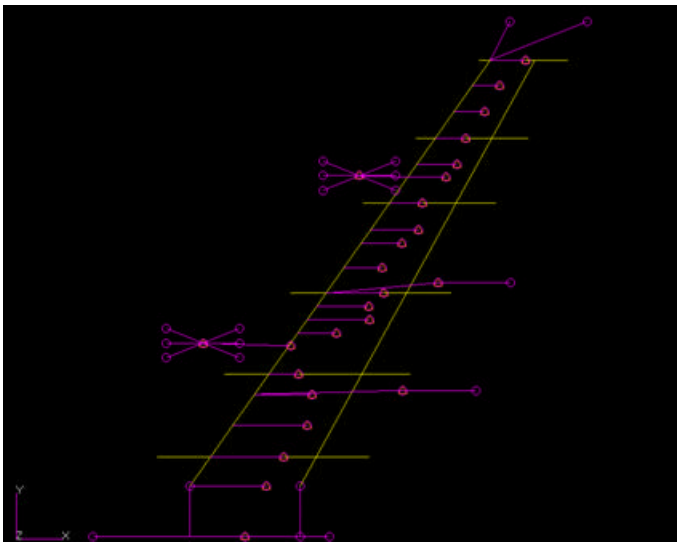

Figure 23. Equivalent Two Spar Wing FE Model

7.2. Results

Two cases were analysed; firstly, using the first three modes as the optimisation objective, and secondly trying to re-create the first five modes of the original wing. The results are shown below alongside the target frequencies.

Case 1 - 3 modes

Target frequencies: 1.6829 3.3127 5.4791[Hz]

Converged frequencies: 1.7893 3.1507 5.5651[Hz]

Percentage difference: 4.9411%

Case 2 - 5 modes

Target frequencies: 1.6829 3.3127 5.4791 6.0044 7.541[Hz]

Converged frequency: 1.5705 3.6555 4.7721 6.6425 8.7635[Hz]

Percentage difference: 10.387%

For the first case it can be seen that the technique works very well at achieving the desired modal properties; the difference between the results and the original wing is less than 5%. As we try to optimise for a greater number of modes (five), the analysis results in a less accurate but still respectable similarity to the original modes (approximately 10% difference).

8. Initial Scaled Model Design

The above optimisation approach is to be used for the design of a half sensorcraft wind tunnel model. This will be used by Lt.Col Vanessa Bond for her studies into the non-linear deflection / buckling behaviour and at Manchester as a bigger demonstrator of the gust load alleviation device.

The full-scale sensorcraft is shown in figure 24 and the internal construction of the proposed wind tunnel model in figure 25. Note that an outer metal skin will be applied as well. The design parameters in the optimisation process will be the spar and rib dimensions and also the skin thickness. It is worth noting that the model wing is attached in all 6 DOF at the wall whereas the rear wall attachment allows some vertical motion via a spring attachment. The two spar and rib construction will be used as it is relatively simple to manufacture and through changing the parameters it should be possible to achieve a scaled model.

One difficulty with implementing the optimisation of the scaling process is that the University of Manchester is not allowed to have access to the full-size FE model and consequently have to rely upon Vanessa Bond at AFIT to perform the required calculations for us.

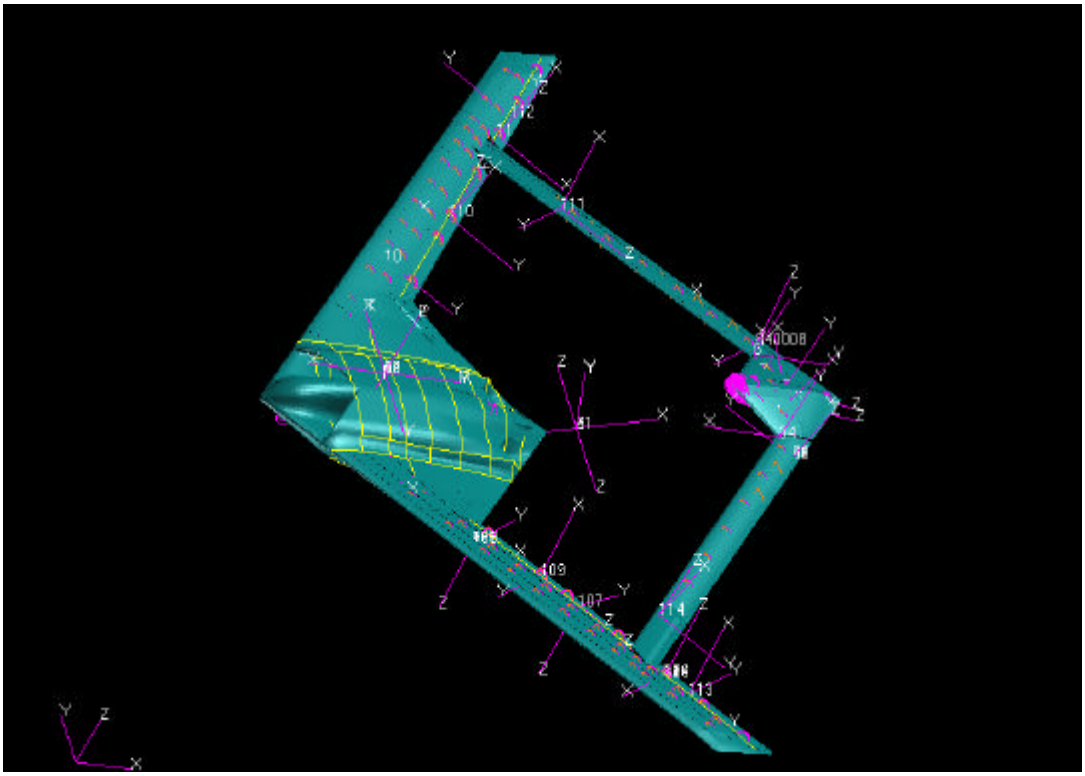

Figure 24. Full-size Sensorcraft Model

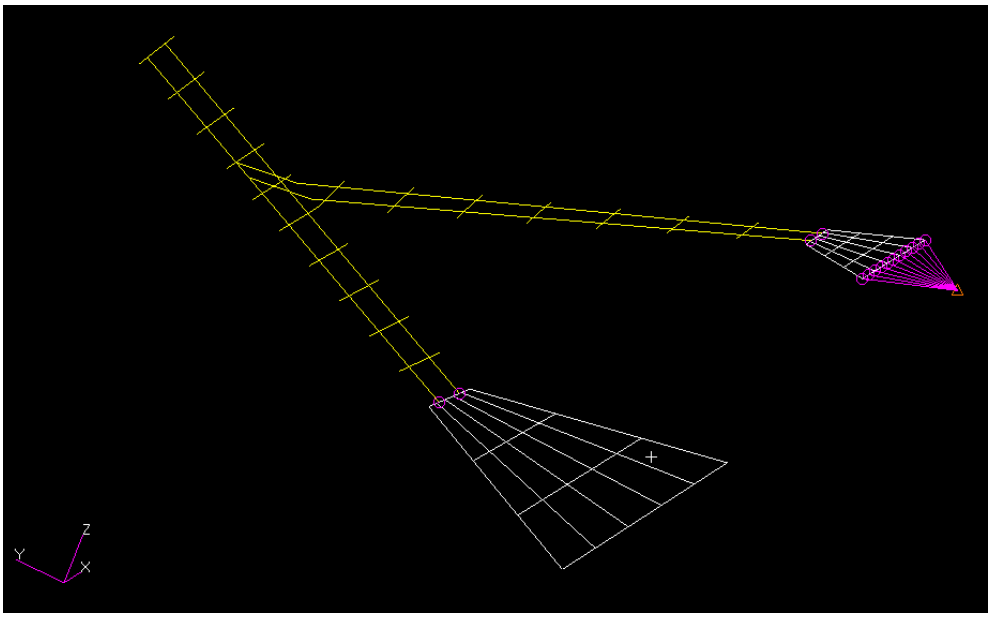

Figure 25. Two Spar Wing Tunnel Model Internal Structure FE Mesh

9. Conclusions

A prototype wind tunnel model of a passive gust load alleviation device has been designed, manufactured and tested. Initial results show that the concept performs as expected. An approach for the aeroelastic scaling of a half sensorcraft model has been defined and a methodology to achieve this demonstrated upon an example wing. This approach will be applied for the design of a half sensorcraft model to be built and tested at Manchester.

10. ACKNOWLEDGMENT

The authors would like to thank the EOARD for its support, and also the technical input from Dr Max Blair, Dr Robert Canfield and Lt.Col Vanessa Bond.

11. REFERENCES

[1] Final Report March 1 2006 EOARD Contract FA8655-05-1-3006
Structural Design and Analysis of an Aeroelastic Tailoring and Passive Load Alleviation Concept for a Sensor Craft Professor J E Cooper, Prof. O. Sensburg, Aizmal Ainul
University of Manchester, UK

[2] Joined Wing Aeroelastic Design with Geometric Non-Linearity – M.Blair, R A Canfield and R W Roberts. Journal of Aircraft v42 n4 pp 832-848 2005

[3] Aeroelasticity – R L Bisplinghoff, H Ashley & R L Halman. Adison Wesley 1955.